Does the Madden-Julian Oscillation Influence Aerosol Variability?

Baijun Tian, Duane E. Waliser, Ralph A. Kahn, Qinbin Li

Jet Propulsion Laboratory, California Institute of Technology, Pasadena, CA

Yuk L. Yung, Tomasz Tyranowski,

Div of Geological and Planetary Sciences, Cal Institute of Technology, Pasadena, CA

Igor V. Geogdzhayev, Michael I. Mishchenko,

NASA Goddard Institute for Space Studies, New York, NY

Omar Torres

Joint Center for Earth Systems Tech., Univ. Maryland Baltimore County, Baltimore, MD

J. Geophys. Res. - Atmospheres

Draft, July 10th, 2007

Corresponding author address: Dr. Baijun Tian, Jet Propulsion Laboratory, M/S 183-501, California Institute of Technology, 4800 Oak Grove Drive, Pasadena, CA 91109. Email: Baijun.Tian@jpl.nasa.gov

Abstract

We investigate the potential modulation of aerosols by the Madden-Julian Oscillation (MJO) using satellite-based global aerosol products, including aerosol index (AI) from the Total Ozone Mapping Spectrometer (TOMS) on Nimbus-7, and aerosol optical thickness (AOT) from the Moderate Resolution Imaging Spectroradiometer (MODIS) on Terra and Aqua and the Advanced Very High Resolution Radiometer (AVHRR) on NOAA satellites. A composite analysis is performed for boreal winter, and the global pentad rainfall data from the NOAA Climate Prediction Center (CPC) Merged Analysis of Precipitation (CMAP) are used to identify MJO events. The composites exhibit large variations in the TOMS AI and MODIS/AVHRR AOT over the equatorial Indian and western Pacific Oceans where MJO convection is active as well as the tropical Africa and Atlantic Ocean where MJO convection is relatively weak but the background aerosol level is relatively high. In particular, the composites exhibit systematic variations in the TOMS AI and MODIS/AVHRR AOT in conjunction with local rainfall variability, especially over the equatorial Indian and western Pacific Oceans. In general, there is a strong inverse linear relationship between the TOMS AI and rainfall anomalies. On the other hand, there is a weaker and less coherent positive correlation between the MODIS/AVHRR AOT and rainfall anomalies. The latter is more consistent with the in-situ Aerosol Robotic Network AOT data at Kaashidoo and Nauru. These results indicate that the MJO and its associated rainfall and circulation variability can systematically influence the aerosol variability. Different sensor sensitivity, cloud clearing, and possible physical mechanisms, such as wet deposition versus aerosol humidity effect, absorbing versus non-absorbing aerosols, and vertical distribution are discussed to explain the

different relationships between the MJO rainfall and aerosol products analyzed here. Suggestions for follow-on research are also discussed.

1. Introduction

Atmospheric aerosols (mainly in the troposphere) play an important role in the climate system and the hydrologic cycle [*IPCC*, 2001; *Ramanathan et al.*, 2001a; *Kaufman et al.*, 2002a; *Yu et al.*, 2006]. First, they interact with solar and thermal radiation (direct effect) by scattering sunlight and reflecting a fraction of it back to space and by absorbing sunlight in the atmosphere in some cases. Thus, aerosols can cool the climate system and surface but may warm the atmosphere [e.g., *Twomey et al.*, 1984; *Charlson et al.*, 1992; *Kiehl and Briegleb*, 1993; *Eck et al.*, 1998; *Satheesh and Ramanathan*, 2000; *Ramanathan et al.*, 2001a]. As a result, aerosols can influence the atmospheric temperature and water vapor profiles and cloud development [e.g., *Hansen et al.*, 1997; *Ackerman et al.*, 2000] and in turn the hydrological cycle [e.g., *Ramanathan et al.*, 2001a]. Second, aerosols influence cloud droplet concentration and size by serving as cloud condensation nuclei (indirect effect) and may cause changes in precipitation patterns, cloud cover, and possibly the frequency of extreme events [e.g., *Rosenfeld*, 1999; *Rosenfeld*, 2000; *Andreae et al.*, 2004; *Koren et al.*, 2004].

Unlike greenhouse gases, such as carbon dioxide and methane, which have long lifetimes and are rather homogeneous in the atmosphere, the spatial and temporal distributions of aerosols are heterogeneous, resulting from their short lifetime (~1 week) owing to wet and dry deposition [*Herman et al.*, 1997; *Husar et al.*, 1997]. Thus, daily global satellite observations and continuous *in-situ* measurements are needed to

document the variability of aerosol amounts and their optical properties over the globe [*King et al.*, 1999; *Kaufman et al.*, 2002a]. However, due to the measurement challenges (e.g., sampling, type, size, vertical structure), the spatial and temporal variability of aerosols has not been comprehensively documented. In particular, to the best of our knowledge, the spatial and temporal patterns of the intraseasonal (30–90 day) variability of aerosols and its connection to the Madden-Julian Oscillation (MJO) have not yet been studied, not to mention in detail on a regional basis.

The MJO (aka Intraseasonal Oscillation) [*Madden and Julian*, 1971; 1994; 2005] is the dominant component of intraseasonal variability in the tropical atmosphere. The MJO is characterized by slowly (~5 m s^{-1}) eastward-propagating, large-scale oscillations in the tropical deep convection and baroclinic wind field, especially over the warmest tropical waters in the equatorial Indian and western Pacific Oceans [*Rui and Wang*, 1990; *Hendon and Salby*, 1994; *Kiladis et al.*, 2001]. Such characteristics tend to be most strongly exhibited during the boreal winter (November-April) when the Indo-Pacific warm pool is centered near the equator. During the boreal summer (May-October), the change in the large-scale circulation associated with the Asian summer monsoon results in the largest-scale aspects of the disturbances propagating more northeastward, from the equatorial Indian Ocean into Southeast Asia [e.g., *Wang and Rui*, 1990; *Waliser*, 2006b]. For more comprehensive reviews of the MJO and related issues, the reader is referred to *Lau and Waliser* [2005].

Since its discovery, the MJO has continued to be a topic of significant interest due to its extensive interactions with other components of the climate system and the fact that it represents a connection between the better-understood weather and the seasonal-to-

95 interannual climate variations. To date, the MJO has been shown to have important
96 influences on various weather and climate phenomena over the globe at many time
97 scales, such as the diurnal cycle of tropical deep convection [e.g., *Johnson et al.*, 1999;
98 *Tian et al.*, 2006a], Asian and Australian monsoon onsets and breaks [e.g., *Yasunari*,
99 1980; *Hendon and Liebmann*, 1990; *Wheeler and McBride*, 2005], El Niño-Southern
100 Oscillation [e.g., *McPhaden*, 1999; *Lau*, 2005], tropical hurricanes [e.g., *Maloney and*
101 *Hartmann*, 2000; *Higgins and Shi*, 2001], extreme precipitation events [e.g., *Higgins et*
102 *al.*, 2000; *Jones et al.*, 2004], and extra-tropical circulation and its weather patterns [e.g.,
103 *Jones*, 2000; *Vecchi and Bond*, 2004]. Furthermore, the large-scale MJO convection,
104 circulation and thermodynamic characteristics have also been relatively well documented
105 and in some cases understood [e.g., *Rui and Wang*, 1990; *Hendon and Salby*, 1994;
106 *Kiladis et al.*, 2001; *Tian et al.*, 2006b]. However, the impact of the MJO on atmospheric
107 composition is only beginning to be documented [e.g., *Ziemke and Chandra*, 2003; *Tian*
108 *et al.*, 2007; *Wong and Dessler*, 2007]. In the present study, we investigate the possible
109 modulation of aerosol variability by the MJO using satellite-based global aerosol
110 products. Important to the implications of this work are the findings and interests
111 regarding the potential predictability of the MJO that extends to 2-4 weeks as indicated
112 by empirical and dynamical studies (e.g. *Waliser* [2006a]). Thus, if the MJO does in fact
113 systematically influence the aerosol variability, then societally relevant prediction of
114 aerosols and air quality with similar lead times may be possible.

115 Section 2 introduces the global satellite aerosol products used for this study, along
116 with the methodology. Our main results are presented in section 3, followed by a
117 summary and discussion in section 4.

2. Data and Methodology

There exist numerous global aerosol products derived from satellite sensors. However, due to the challenge of retrieving aerosol parameters from top-of-atmosphere radiances, including issues related to sensor calibration, cloud screening, corrections for surface reflectivity and variability of aerosol properties (size distribution, refractive index, etc) [*King et al.*, 1999], substantial differences exist among the existing global aerosol products [*Myhre et al.*, 2004; *Jeong and Li*, 2005b; *Jeong et al.*, 2005; *Myhre et al.*, 2005]. For this study, we use three satellite-based global aerosol products: Total Ozone Mapping Spectrometer (TOMS) Aerosol Index (AI), Moderate Resolution Imaging Spectroradiometer (MODIS) aerosol optical thickness (AOT), and Global Aerosol Climatology Project (GACP)/Advanced Very High Resolution Radiometer (AVHRR) AOT.

The TOMS AI used here are the daily AI (level 3, version 8) on a resolution 1º × 1.25º latitude-longitude made by Nimbus-7 TOMS from January 1980 to December 1992 [*Herman et al.*, 1997]. Currently the AI is calculated from observations by the Ozone Monitoring Instrument (OMI) aboard the Aura satellite [*Torres et al.*, 2007]. The AI is calculated from the ratio of ultraviolet (UV) radiance measurements at 0.331 and 0.360 μm and can detect the presence of aerosols that absorb UV radiation over both ocean and land [*Hsu et al.*, 1996; *Herman et al.*, 1997] and even over very bright surfaces like clouds and ice/snow [*Hsu et al.*, 1999a]. The AI is most sensitive to UV-absorbing aerosols such as mineral dust, elevated biomass burning smoke and volcanic ash, and is insensitive to non-absorbing aerosols, such as sea salt and sulfuric acid aerosols [*Torres et al.*, 1998; *de Graaf et al.*, 2005]. Furthermore, the AI is highly dependent on the

141 altitude of the aerosol layer and cannot detect biomass burning aerosols in the lower
142 troposphere, below about 2 km [*Hsu et al.*, 1999b; *de Graaf et al.*, 2005]. The magnitude
143 of the AI depends on aerosol parameters, such as AOT, single-scattering albedo, and
144 asymmetry parameter, and surface albedo. In particular, the AI increases linearly with
145 AOT, with a slope proportional to the aerosol single-scattering albedo [*Torres et al.*,
146 1998; *de Graaf et al.*, 2005]. Since soot containing aerosols also absorb in the visible and
147 near infrared, the AI can be regarded as a proxy of aerosol absorption by carbon-
148 containing aerosols.

149 MODIS, aboard the NASA Earth Observing System's Terra and Aqua satellites
150 (crossing the equator in opposite directions on the day side at about 10:30 and 13:30 local
151 time, respectively), performs near global, daily observations of atmospheric aerosols.
152 MODIS has 36 channels ranging from 0.44 to 15 μm. Seven of these channels between
153 0.47 and 2.13 μm are used to retrieve aerosol properties over cloud and surface-screened
154 areas identified by using other channels and examining spatial variability [*Martins et al.*,
155 2002; *Li et al.*, 2004]. The MODIS aerosol product is generated using different retrieval
156 algorithms over ocean and land. The over-ocean algorithm was originally documented by
157 *Tanre et al*. [1997] and updated by *Levy et al.* [2003] and *Remer et al.* [2005]. It utilizes
158 calibrated radiances observed in six bands (nominal wavelengths of 0.55, 0.66, 0.87,
159 1.24, 1.64, and 2.13 μm) at a spatial resolution of 500 m under clear-sky conditions
160 determined by a dedicated cloud-masking algorithm [*Martins et al.*, 2002]. Because of its
161 wide spectral range and the greater simplicity of the ocean surface, the MODIS retrieved
162 AOT over ocean has greater accuracy, i.e., ±0.03±0.05AOT [*Remer et al.*, 2002; *Levy et*
163 *al.*, 2003; 2005; *Remer et al.*, 2005]. The algorithm over land was originally documented

by *Kaufman et al*. [1997] and updated by *Remer et al.* [2005]. It utilizes calibrated radiances observed in three bands (nominal wavelengths of 0.47, 0.66, and 2.13 μm). Over vegetated land, MODIS retrieves AOT with high accuracy, i.e., ±0.05±0.2AOT [*Chu et al.*, 2002; *Remer et al.*, 2005]. The MODIS AOT employed in this study is reported at 0.55 μm. The data is version 4 of the MOD08 data set (L3 atmosphere product) with a spatial resolution of 1º × 1º from 24 February 2000 to 9 December 2005.

The GACP/AVHRR (hereafter AVHRR) aerosol product [*Mishchenko et al.*, 1999; *Geogdzhayev et al.*, 2002; *Mishchenko and Geogdzhayev*, 2007] (updated at http://gacp.giss.nasa.gov/) contains the daily mean AOT at 0.55 μm from 1 January 1982 to 30 June 2005 over ocean. The product resolution is 1º × 1º on an equal-angle grid. It was derived from clear-sky calibrated radiances from AVHRR channel 1 (nominal wavelength, λ = 0.63 μm) and channel 2 (λ = 0.85 μm) contained in the International Satellite Cloud Climatology Project (ISCCP) DX data set [*Rossow and Schiffer*, 1999]. Aerosol particles are assumed to be spherical, as in the MODIS AOT retrieval. A modified power law size distribution was adopted with the aerosol refractive indices fixed at m = 1.5–0.003i. The shaping factor, which is the parameter that determines the shape of the modified power law size distribution, has a unique relationship with the Angstrom exponent and the effective radius of aerosols. Possible sources of errors in the AVHRR aerosol retrievals, as with other passive satellite aerosol retrievals, are radiance calibration, cloud screening, the assumptions about aerosols and uncertainties in boundary conditions and water vapor absorption at channel 2 [*Mishchenko et al.*, 1999; *Geogdzhayev et al.*, 2002; *Mishchenko and Geogdzhayev*, 2007].

To help validate and understand the relationships between the MJO rainfall and

187 satellite aerosol products, we use the V2.0, L2.0 (cloud-screened and quality-assured)
188 daily Aerosol Robotic Network (AERONET) AOT at Kaashidoo (73.5ºE, 4.9ºN) and
189 Nauru (167ºE, 0.5ºS). The AERONET program [*Holben et al.*, 1998; 2001] is a federated
190 ground-based aerosol measurement network using automatic sun and sky scanning
191 spectral radiometers. AERONET includes about 200 sites around the world, covering all
192 major tropospheric aerosol regimes. Spectral radiance measurements are calibrated and
193 screened for cloud-free conditions [*Smirnov et al.*, 2000]. The program provides quality-
194 assured aerosol optical properties to assess and validate satellite retrievals. The
195 AERONET AOT data used here from Kaashidoo were taken between 20 February 1998
196 and 11 July 2000 and those for Nauru are from 15 June 1999 to 11 June 2006.

197 To identify MJO events, we use global pentad (i.e., 5-day average) rainfall data
198 from the NOAA Climate Prediction Center (CPC) Merged Analysis of Precipitation
199 [CMAP, *Xie and Arkin*, 1997] from 1 Jan 1979 to 31 May 2006 on a 2.5º×2.5º grid. For
200 the MJO analysis and composite procedure, we use the approach described in previous
201 work [e.g., *Waliser et al.*, 2003; *Tian et al.*, 2006b]. Briefly, all the data were first binned
202 into pentad values. Intraseasonal anomalies were obtained by removing the annual cycle
203 and then band-pass filtering (30–90 day) the data. To isolate the dominant structure of the
204 MJO, an extended empirical orthogonal function (EEOF) was applied using time lags of
205 ±5 pentads (i.e. 11 pentads total) on boreal winter rainfall for the region 30ºS-30ºN and
206 30ºE-150ºW (see Figure 1 in *Tian et al*. [2006b]). Next, MJO events were chosen based
207 on the amplitude time series of the first EEOF mode of the rainfall anomaly. Figure 1
208 shows the dates and number of the selected MJO events, along with an indication of their
209 relative amplitudes. For each selected MJO event, the corresponding 11-pentad rainfall,

AI or AOT anomalies were extracted for each data set (TOMS, MODIS, AVHRR, and AERONET). A composite MJO cycle (11 pentads) of anomalies was then obtained by averaging the selected MJO events.

3. Results

Figure 2 shows the horizontal maps of the TOMS AI anomalies for the composite MJO cycle with 95% confidence limits applied based on a Student's t-test. For simplicity, only lags ±4, ±2, and 0 pentads of the MJO cycle are shown. Contour plots overlaid on the color shadings are the corresponding MJO composite rainfall anomalies. As expected, these closely mimic the space-time variations exhibited by the EEOF patterns (see Figure 1 in *Tian et al.* [2006b]). The AI anomalies range up to about ±0.6 for the *composite* MJO but about ±2 for individual events. This indicates that intraseasonal variations of AI are significant and comparable to those associated with the annual cycle and interannual variability [e.g., *Herman et al.*, 1997; *Cakmur et al.*, 2001; *Mahowald et al.*, 2003]. Figure 2 shows that significant AI anomalies are found in the tropical Indian and western Pacific Oceans where the MJO convection is active. Evident in Figure 2 is the close association between negative AI anomalies and positive rainfall anomalies and vice versa. The zero-lag correlation between AI and rainfall is shown in Figure 4 (top), which demonstrates a strong negative correlation between TOMS AI and rainfall in the tropical Indian and western Pacific Oceans. This relationship seems to be consistent with the seasonal study of *Lau and Kim* [2006], who shows a decrease of TOMS AI after the Indian summer monsoon was established (high rainfall) (their Figure 2). Over equatorial Africa and Atlantic Ocean where MJO convection is relatively weak, equally large AI anomalies are also found in conjunction with relatively weak rainfall anomalies from the

MJO. The correlation between AI and rainfall is also negative over this region albeit much weaker. The large AI anomalies over this region may be due to the large background AI, that is, high absorbing aerosol loading due to Sahara desert dust and biomass burning smoke from South Africa [*Herman et al.*, 1997].

Similar diagram to Figure 2 but for the MODIS AOT is shown in Figure 3. The MODIS AOT anomalies range up to about ±0.02 for the *composite* MJO but about ±0.1 for individual events. These intraseasonal variations are large compared to its background mean (~0.2) [*Myhre et al.*, 2004; *Jeong et al.*, 2005; *Myhre et al.*, 2005]. Similar to TOMS AI, significant MODIS AOT anomalies are also found in the tropical Indian and western Pacific Oceans as well as equatorial Africa and Atlantic Ocean. However, the relationship between MODIS AOT and rainfall is less coherent than for TOMS AI. In general, in the tropical Indian and western Pacific Oceans where the MJO convection is active, positive AOT anomalies tend to be associated with positive rainfall anomalies and vice versa. This is also confirmed by a weak positive correlation between MODIS AOT and rainfall in this region (Figure 4, middle). Our results appear to be consistent with the positive correlation between the MODIS AOT and cloud cover found by *Kaufman et al.* [2002b] and *Lin et al.* [2006].

The spatial and temporal pattern of the AVHRR AOT anomalies is similar to that from MODIS but even less coherent than MODIS (not shown). This is probably due to the poorer spatial coverage of the daily AVHRR AOT data and its smaller "dynamic range" than MODIS. More conservative cloud screening algorithms were applied by *Mishchenko et al.* [1999] and *Geogdzhayev et a*l. [2002], in addition to the ISCCP cloud detection algorithm [*Rossow and Garder*, 1993]. The additional cloud screening aims to

256 eliminate small cumulus clouds and optically thin cirrus clouds. However, the strict cloud
257 masking may have an adverse impact of discarding real aerosol signals by misclassifying
258 them as clouds [*Husar et al.*, 1997; *Haywood et al.*, 2001]. For instance, an AOT
259 threshold of 2 is used for the GACP/AVHRR product as a part of cloud screening, which
260 will discard some cases with heavy aerosol loading [*Mishchenko and Geogdzhayev*,
261 2007]. The less coherent AVHRR AOT MJO variability is also supported by an even
262 weaker, relative to MODIS, positive correlation between AVHRR AOT and rainfall
263 (Figure 4, bottom). Our results appear to be consistent with the positive correlation
264 between the AVHRR AOT and cloud cover found by *Ignatov and Nalli* [2002] and
265 *Ignatov et al.* [2004].

266 To help understand the above (apparent) discrepancy in the satellite-observed
267 aerosol anomalies associated with the MJO, the relationship between the composite
268 AERONET AOT and rainfall anomalies is examined at Kaashidoo and Nauru (Figure 5).
269 We choose the AERONET AOT at 0.50 μm, which is close to the channel used by
270 MODIS and AVHRR, but the results for other channels are similar (not shown). For
271 comparison, time series from the composite TOMS AI, MODIS AOT, and AVHRR AOT
272 near these two sites are also shown in Figure 5. Consistent with the discussion above, the
273 TOMS AI is negatively correlated with rainfall, while the MODIS/AVHRR AOT is
274 positively correlated with rainfall at both Kaashidoo and Nauru. Figure 5 indicates that
275 there exists a strong positive correlation (correlation coefficient ~ +0.70 for Kaashidoo
276 and +0.90 for Nauru) between the AERONET AOT and rainfall anomalies at both
277 Kaashidoo and Nauru. This aerosol-rainfall relationship appears to be consistent with the
278 positive correlation between AERONET AOT and cloud cover found by *Jeong and Li*

[2005a]. Furthermore, the magnitude of the AERONET AOT anomalies (~0.02) is also comparable to the MODIS/AVHRR AOT anomalies. Thus, the AERONET data seem to support the weak positive correlation between MODIS/AVHRR AOT and rainfall anomalies as shown in Figures 3 & 4.

4. Summary and Discussion

We investigated the possible modulation of the aerosol variability by the MJO using satellite-based global aerosol products, specifically, the TOMS AI, MODIS AOT, and AVHRR AOT. Our results indicate that the intraseasonal aerosol variability is large and comparable to those associated with annual cycle and interannual variability. Large variations in the TOMS AI, MODIS AOT and AVHRR AOT are mainly found over the equatorial Indian and western Pacific Oceans where MJO convection is active as well as the tropical Africa and Atlantic Ocean where MJO convection is relatively weak but the background aerosol level is relatively high. In particular, there is a systematic relationship between the TOMS AI, MODIS AOT, and AVHRR AOT anomalies and the MJO rainfall anomalies over the equatorial Indian and western Pacific Oceans. During the wet phase of the MJO, TOMS AI decreases, whereas MODIS and AVHRR AOT increase, in association with the enhanced precipitation, cloud cover and water vapor in the atmosphere and vice versa. Thus, there is a strong negative correlation between the TOMS AI and rainfall anomalies but a weaker and less coherent positive correlation between the MODIS AOT, AVHRR AOT and rainfall anomalies. The latter is more consistent with the in-situ AERONET AOT data, which also show a strong positive correlation between AERONET AOT and rainfall anomalies at both Kaashidoo and Nauru. These results indicate that the MJO and its associated rainfall and circulation

variability systematically influence remote-sensing-retrieved aerosol variability.

These findings raise a number of interesting questions. First, are these aerosol-rainfall relationships physical or is one or more of them a result of the aerosol sampling and retrieval artifacts? Cloud screening is a major issue for the satellite aerosol retrievals, and has been posited as a possible reason for the positive correlation between AOT and rainfall/cloud cover because cloud-associated mechanisms can alias the aerosol retrievals [*Myhre et al.*, 2004; *Jeong and Li*, 2005a; 2005b; *Jeong et al.*, 2005; *Kaufman et al.*, 2005; *Myhre et al.*, 2005]. The options include unscreened sub-pixel clouds, cloud-scattered light in broken cloud regions misidentified as high AOT. However, since MODIS, AVHRR and AERONET all show a positive correlation between AOT and rainfall/cloud cover despite the differences in cloud clearing algorithms among them, this appears to suggest that this positive correlation may be real. Also, since TOMS AI can only retrieve aerosol above the cloud top, it should be kept in mind that smaller TOMS AI values in the enhanced phase of the MJO may be due to increased occurrence of high clouds. Nevertheless, since both seasonal study by *Lau and Kim* [2006] and this study of the intraseasonal time scale indicate a similar relationship, the negative correlation between the TOMS AI and the MJO rainfall may indicate a real physical modulation of aerosols by the MJO.

Second, if the relationships between the MJO rainfall and aerosol products analyzed here do indicate true aerosol processes, then why is there a negative correlation between the TOMS AI and rainfall anomalies in contrast to a positive correlation between the MODIS/AVHRR AOT and rainfall anomalies? Please note that the TOMS AI is most sensitive to absorbing aerosols and those in the upper troposphere and very

insensitive to non-absorbing aerosols especially those in the boundary layer [*Torres et al.*, 1998; *de Graaf et al.*, 2005]. On the other hand, the MODIS and AVHRR AOT are sensitive to both absorbing and non-absorbing aerosols and aerosols in both upper and lower troposphere. Thus, the different relationships between the satellite aerosol products and rainfall may be due to the different aerosol optical properties of absorbing versus non-absorbing aerosols and upper versus lower tropospheric aerosols. As a result, the outstanding question needs to be answered is: What is the relative contribution of wet deposition versus aerosol humidity effect (AHE), absorbing versus non-absorbing aerosols, upper versus lower tropospheric aerosols in these relationships?

It is well known that rainfall is a most efficient aerosol removal mechanism through wet deposition [e.g., *Koch et al.*, 2003; *Wilcox and Ramanathan*, 2004]. In the wet phase of the MJO, the precipitation is significantly enhanced and this can increase the wet deposition for both absorbing and non-absorbing aerosols and reduce the aerosol mass loading in the troposphere. The opposite is true for the dry phase of the MJO. Thus, we would expect a negative correlation between the tropospheric aerosol mass loading and the rainfall if wet deposition is the dominant mechanism determining the aerosol variability in the intraseasonal time scale. The negative correlation between the TOMS AI, an indicator of absorbing aerosol mass loading, and rainfall is consistent with this physical mechanism and may indicate the importance role of wet deposition. However, the positive correlation between MODIS/AVHRR AOT and rainfall cannot be explained by the wet deposition mechanism alone. This implies that other physical mechanisms in addition to the wet deposition must be important to determining the aerosol variability in the intraseasonal time scale.

Please note that AOT is a vertically integrated (column) quantity measuring the magnitude of aerosol extinction (due to scattering and absorption). The AOT depends on aerosol mass loading, scattering, and absorption efficiencies that are further linked with aerosol size distribution and composition. Therefore any factors affecting the size distribution will impact the optical properties. One critical factor is the relative humidity (RH). Some aerosol types are hygroscopic, meaning that they grow as they take up water vapor. As a result, their size increases and their refractive indices change, in turn leading to changes in their optical properties, especially the scattering coefficient. This strong dependence of scattering AOT on the atmospheric RH is referred to as AHE [e.g., *Jeong et al.*, 2007 and references in]. For example, the scattering cross section of sulfate-dominated aerosol doubles as RH increases from 40% to 80% [*Hobbs et al.*, 1997; *Kaufman et al.*, 1998]. On the other hand, the response of the absorption coefficient to increasing RH is uncertain, although theoretical studies indicate it should be much smaller than that for the scattering coefficient [*Redemann et al.*, 2001]. Consequently, for hygroscopic aerosols, single-scattering albedo and asymmetry factor increase with RH. Tropospheric RH is much higher in the wet phase of the MJO (~80%) than its dry phase (~30%) [e.g., *Chen et al.*, 1996; *Lin and Johnson*, 1996]. Thus, we should expect a positive correlation between the scattering AOT and the MJO rainfall in contrast to a weaker and/or no correlation between the absorbing AOT and the MJO rainfall if the AHE is the dominant mechanism determining the AOT variability in the intraseasonal time scale. Therefore, the positive correlation between the rainfall and MODIS/AVHRR AOT (a measure of aerosol scattering effect), in contrast to the negative correlation between the rainfall and TOMS AI (a measure of aerosol absorption effect) may indicate

371 the fundamental role of AHE in influencing the intraseasonal AOT variability.

372 In addition, the different relationships between the MJO rainfall and aerosol
373 products may imply different aerosol variability at different vertical levels because the
374 TOMS AI is most sensitive to the absorbing aerosols in the upper troposphere [*Hsu et al.*,
375 1999b; *de Graaf et al.*, 2005], while the MODIS/AVHRR AOT can measure the aerosols
376 in both upper and lower troposphere. For example, the stronger near-surface winds
377 associated with the westerly wind bursts during the wet phase of the MJO [e.g., *Kiladis et*
378 *al.*, 1994; 2005] may generate more bright, near-surface sea salts. These strong scattering
379 sea salts in the lower troposphere can be detected by both MODIS and AVHRR AOT but
380 invisible to the TOMS AI. Thus, we should expect a positive correlation between the
381 MODIS AOT, AVHRR AOT and rainfall but no relationship between the TOMS AI and
382 rainfall if the surface wind variability associated with the MJO can influence the over-
383 ocean aerosol variability.

384 The findings and discussions above indicate a strong but complex relationship
385 between the MJO and the aerosol variability. In particular, many physical or non-physical
386 mechanisms, such as different sensor sensitivity, cloud clearing, wet deposition, aerosol
387 humidity effect, absorbing versus non-absorbing aerosols, and vertical distribution, may
388 work together to determine the different relationships between the MJO rainfall and
389 aerosol products analyzed here. Coupled with the potential to predict the MJO with lead
390 times up to 2-4 weeks [*Waliser*, 2006a], along with the potential impacts of aerosol on
391 cloud processes [e.g., *Ramanathan et al.*, 2001a; *Andreae et al.*, 2004; *Koren et al.*,
392 2004], suggests an important need to more completely document the aerosol intraseasonal
393 variability as well as to further investigate the complex mechanisms behind the MJO

394 rainfall and aerosol relationship. For example, further investigation is needed for the
395 above hypotheses regarding wet deposition versus AHE, absorbing versus non-absorbing
396 aerosols, and upper versus lower tropospheric aerosols in this complex aerosol-rainfall
397 relationship. To that end, a synergetic approach combining multi-sensor satellite data
398 analysis, targeted aircraft observations, and state-of-the-art chemistry-transport modeling
399 together may be required. For example, we can analyze aerosol particle information, such
400 as single-scattering albedo or Angstrom exponent from AERONET to quantify the role of
401 AHE and absorbing versus non-absorbing aerosols in this relationship. However,
402 AERONET only retrieves a column-effective single-scattering albedo and is not as
403 reliable as the AERONET AOT. Also, it is only valid for AOT>0.4 and does not
404 distinguish among different aerosol modes within the total column. Thus, the usefulness
405 of analyzing the single-scattering albedo from AERONET may be limited. Although the
406 coverage frequency of the Multi-angle Imaging Spectroradiometer (MISR) [*Diner et al.*,
407 1998] may be too coarse for the MJO study – owing to its narrow swath – there may still
408 be useful aerosol size information over land regions for this purpose which is a relative
409 strength of MISR [*Martonchik et al.*, 2002; *Kahn et al.*, 2005]. Furthermore, although the
410 data record is still relatively short, it should be possible to utilize the vertical aerosol
411 profile from Cloud-Aerosol Lidar and Infrared Pathfinder Satellite Observations
412 (CALIPSO) [*Winker et al.*, 2003; 2004], which is lacking for the TOMS AI, MODIS
413 AOT, and AVHRR AOT, to better understand how the vertical distribution of aerosols
414 may influence the sampling characteristics of the TOMS AI, MODIS AOT, and AVHRR
415 AOT and the MJO rainfall-aerosol relationship we found here. However, due to the
416 inherent limitations of satellite- and/or ground-based remote-sensed aerosol products,

such as cloud clearing and sensor calibration, coordinated aircraft aerosol measurements from intensive field campaigns, such as Indian Ocean Experiment (INDOEX) [*Ramanathan et al.*, 2001b], Asian Pacific Regional Aerosol Characterization Experiment (ACE-Asia) [*Huebert et al.*, 2003; *Seinfeld et al.*, 2004], and Asian Brown Clouds (ABC) [*Ramanathan et al.*, 2005] may be needed. Also, these target aircraft measurements will also be useful to test the reliability of chemistry-transport models in representing the MJO rainfall-aerosol relationship. At last, if the chemistry-transport models can realistically capture this MJO rainfall-aerosol relationship, we can use the models to fully understand the aerosol-rainfall relationship and physical, chemical and radiative mechanisms behind this complex relationship.

Acknowledgements

This research was carried out at the Jet Propulsion Laboratory (JPL), California Institute of Technology (Caltech), under a contract with NASA. B. Tian and D. Waliser were jointly supported by the Research and Technology Development program, Human Resources Development fund, the NASA Modeling, Analysis and Prediction Program, and the AIRS project at JPL. The work of R. Kahn is supported in part by NASA's Climate and Radiation Research and Analysis Program, under H. Maring, and in part by the EOS-MISR instrument project. Y. Yung was supported by NASA grant NNG04GD76G to Caltech and T. Tyranowski acknowledged support by the Caltech SURF program in 2006.

References

Ackerman, A. S., O. B. Toon, D. E. Stevens, A. J. Heymsfield, V. Ramanathan, and E. J. Welton (2000), Reduction of tropical cloudiness by soot, *Science*, *288*, 1042-1047.

Andreae, M. O., D. Rosenfeld, P. Artaxo, A. A. Costa, G. P. Frank, K. M. Longo, and M. A. F. Silva-Dias (2004), Smoking rain clouds over the Amazon, *Science*, *303*, 1337-1342.

Cakmur, R. V., R. L. Miller, and I. Tegen (2001), A comparison of seasonal and interannual variability of soil dust aerosols over the Atlantic ocean as inferred by the TOMS AI and AVHRR AOT retrievals, *Journal of Geophysical Research-Atmospheres*, *106*, 18287-18303.

Charlson, R. J., S. E. Schwartz, J. M. Hales, R. D. Cess, J. A. Coakley, J. E. Hansen, and D. J. Hofmann (1992), Climate forcing by anthropogenic aerosols, *Science*, *255*, 423-430.

Chen, S. S., R. A. Houze, and B. E. Mapes (1996), Multiscale variability of deep convection in relation to large-scale circulation in TOGA COARE, *Journal of the Atmospheric Sciences*, *53*, 1380-1409.

Chu, D. A., Y. J. Kaufman, C. Ichoku, L. A. Remer, D. Tanre, and B. N. Holben (2002), Validation of MODIS aerosol optical depth retrieval over land, *Geophysical Research Letters*, *29*, 1617, doi:10.1029/2001GL013205.

de Graaf, M., P. Stammes, O. Torres, and R. B. A. Koelemeijer (2005), Absorbing aerosol index: Sensitivity analysis, application to GOME and comparison with TOMS, *Journal of Geophysical Research-Atmospheres*, *110*, D01201, doi:10.1029/2004JD005178.

Diner, D. J., J. C. Beckert, T. H. Reilly, C. J. Bruegge, J. E. Conel, R. A. Kahn, J. V. Martonchik, T. P. Ackerman, R. Davies, S. A. W. Gerstl, H. R. Gordon, J. P.

463 Muller, R. B. Myneni, P. J. Sellers, B. Pinty, and M. M. Verstraete (1998), Multi-
464 angle imaging spectroradiometer (MISR) - instrument description and experiment
465 overview, *IEEE Transactions on Geoscience and Remote Sensing*, *36*, 1072-1087.
466 Eck, T. F., B. N. Holben, I. Slutsker, and A. Setzer (1998), Measurements of irradiance
467 attenuation and estimation of aerosol single scattering albedo for biomass burning
468 aerosols in Amazonia, *Journal of Geophysical Research-Atmospheres*, *103*,
469 31865-31878.
470 Geogdzhayev, I. V., M. I. Mishchenko, W. B. Rossow, B. Cairns, and A. A. Lacis (2002),
471 Global two-channel AVHRR retrievals of aerosol properties over the ocean for
472 the period of NOAA-9 observations and preliminary retrievals using NOAA-7
473 and NOAA-11 data, *Journal of the Atmospheric Sciences*, *59*, 262-278.
474 Hansen, J., M. Sato, and R. Ruedy (1997), Radiative forcing and climate response,
475 *Journal of Geophysical Research-Atmospheres*, *102*, 6831-6864.
476 Haywood, J. M., P. N. Francis, I. Geogdzhayev, M. Mishchenko, and R. Frey (2001),
477 Comparison of Saharan dust aerosol optical depths retrieved using aircraft
478 mounted pyranometers and 2-channel AVHRR algorithms, *Geophysical Research*
479 *Letters*, *28*, 2393-2396.
480 Hendon, H. H., and B. Liebmann (1990), The intraseasonal (30-50 day) oscillation of the
481 Australian summer monsoon, *Journal of the Atmospheric Sciences*, *47*, 2909-
482 2923.
483 Hendon, H. H., and M. L. Salby (1994), The life-cycle of the Madden-Julian oscillation,
484 *Journal of the Atmospheric Sciences*, *51*, 2225-2237.
485 Herman, J. R., P. K. Bhartia, O. Torres, C. Hsu, C. Seftor, and E. Celarier (1997), Global
486 distribution of UV-absorbing aerosols from Nimbus-7/TOMS data, *Journal of*
487 *Geophysical Research-Atmospheres*, *102*, 16911-16922.
488 Higgins, R. W., J. K. E. Schemm, W. Shi, and A. Leetmaa (2000), Extreme precipitation
489 events in the western United States related to tropical forcing, *Journal of Climate*,

490 *13*, 793-820.
491 Higgins, R. W., and W. Shi (2001), Intercomparison of the principal modes of
492 interannual and intraseasonal variability of the North American monsoon system,
493 *Journal of Climate*, *14*, 403-417.
494 Hobbs, P. V., J. S. Reid, R. A. Kotchenruther, R. J. Ferek, and R. Weiss (1997), Direct
495 radiative forcing by smoke from biomass burning, *Science*, *275*, 1776-1778.
496 Holben, B. N., T. F. Eck, I. Slutsker, D. Tanre, J. P. Buis, A. Setzer, E. Vermote, J. A.
497 Reagan, Y. J. Kaufman, T. Nakajima, F. Lavenu, I. Jankowiak, and A. Smirnov
498 (1998), AERONET - a federated instrument network and data archive for aerosol
499 characterization, *Remote Sensing of Environment*, *66*, 1-16.
500 Holben, B. N., D. Tanre, A. Smirnov, T. F. Eck, I. Slutsker, N. Abuhassan, W. W.
501 Newcomb, J. S. Schafer, B. Chatenet, F. Lavenu, Y. J. Kaufman, J. V. Castle, A.
502 Setzer, B. Markham, D. Clark, R. Frouin, R. Halthore, A. Karneli, N. T. O'Neill,
503 C. Pietras, R. T. Pinker, K. Voss, and G. Zibordi (2001), An emerging ground-
504 based aerosol climatology: Aerosol optical depth from AERONET, *Journal of*
505 *Geophysical Research-Atmospheres*, *106*, 12067-12097.
506 Hsu, N. C., J. R. Herman, P. K. Bhartia, C. J. Seftor, O. Torres, A. M. Thompson, J. F.
507 Gleason, T. F. Eck, and B. N. Holben (1996), Detection of biomass burning
508 smoke from TOMS measurements, *Geophysical Research Letters*, *23*, 745-748.
509 Hsu, N. C., J. R. Herman, J. F. Gleason, O. Torres, and C. J. Seftor (1999a), Satellite
510 detection of smoke aerosols over a snow/ice surface by TOMS, *Geophysical*
511 *Research Letters*, *26*, 1165-1168.
512 Hsu, N. C., J. R. Herman, O. Torres, B. N. Holben, D. Tanre, T. F. Eck, A. Smirnov, B.
513 Chatenet, and F. Lavenu (1999b), Comparisons of the TOMS aerosol index with
514 sun-photometer aerosol optical thickness: Results and applications, *Journal of*
515 *Geophysical Research-Atmospheres*, *104*, 6269-6279.
516 Huebert, B. J., T. Bates, P. B. Russell, G. Y. Shi, Y. J. Kim, K. Kawamura, G.

517 Carmichael, and T. Nakajima (2003), An overview of ACE-Asia: Strategies for
518 quantifying the relationships between Asian aerosols and their climatic impacts,
519 *Journal of Geophysical Research-Atmospheres*, *108*, 8633,
520 doi:10.1029/2003JD003550.
521 Husar, R. B., J. M. Prospero, and L. L. Stowe (1997), Characterization of tropospheric
522 aerosols over the oceans with the NOAA advanced very high resolution
523 radiometer optical thickness operational product, *Journal of Geophysical*
524 *Research-Atmospheres*, *102*, 16889-16909.
525 Ignatov, A., and N. R. Nalli (2002), Aerosol retrievals from the multiyear multisatellite
526 AVHRR pathfinder atmosphere (PATMOS) dataset for correcting remotely
527 sensed sea surface temperatures, *Journal of Atmospheric and Oceanic*
528 *Technology*, *19*, 1986-2008.
529 Ignatov, A., J. Sapper, S. Cox, I. Laszlo, N. R. Nalli, and K. B. Kidwell (2004),
530 Operational aerosol observations (AEROBS) from AVHRR/3 on board NOAA-
531 KLM satellites, *Journal of Atmospheric and Oceanic Technology*, *21*, 3-26.
532 IPCC (2001), *Climate change 2001: The scientific basis. Contribution of working group*
533 *I to the third assessment report of the intergovernmental panel on climate change*,
534 Edited by J. T. Houghton, Y. Ding, D. J. Griggs, M. Noguer, P. J. van der Linden,
535 X. Dai, K. Maskell and C. A. Johnson, pp 881, Cambridge University Press,
536 Cambridge, UK and New York, NY, USA.
537 Jeong, M.-J., and Z. Q. Li (2005a), Real effect or artifact of cloud cover on aerosol
538 optical thickness, Paper presented at Fifteenth ARM Science Team Meeting,
539 Daytona Beach, Florida, March 14-18, 2005.
540 Jeong, M.-J., Z. Q. Li, E. Andrews, and S.-C. Tsay (2007), Effect of aerosol
541 humidification on the column aerosol optical thickness over the atmospheric
542 radiation measurement southern Great Plains site, *Journal of Geophysical*
543 *Research-Atmospheres*, *112*, D10202, doi:10.1029/2006JD007176.

544 Jeong, M. J., and Z. Q. Li (2005b), Quality, compatibility, and synergy analyses of global
545 aerosol products derived from the advanced very high resolution radiometer and
546 total ozone mapping spectrometer, *Journal of Geophysical Research-*
547 *Atmospheres*, *110*, D10S08, doi:10.1029/2004JD004647.
548 Jeong, M. J., Z. Q. Li, D. A. Chu, and S. C. Tsay (2005), Quality and compatibility
549 analyses of global aerosol products derived from the advanced very high
550 resolution radiometer and moderate resolution imaging spectroradiometer,
551 *Journal of Geophysical Research-Atmospheres*, *110*, D10S09,
552 doi:10.1029/2004JD004648.
553 Johnson, R. H., T. M. Rickenbach, S. A. Rutledge, P. E. Ciesielski, and W. H. Schubert
554 (1999), Trimodal characteristics of tropical convection, *Journal of Climate*, *12*,
555 2397-2418.
556 Jones, C. (2000), Occurrence of extreme precipitation events in California and
557 relationships with the Madden-Julian oscillation, *Journal of Climate*, *13*, 3576-
558 3587.
559 Jones, C., D. E. Waliser, K. M. Lau, and W. Stern (2004), Global occurrences of extreme
560 precipitation and the Madden-Julian oscillation: Observations and predictability,
561 *Journal of Climate*, *17*, 4575-4589.
562 Kahn, R. A., B. J. Gaitley, J. V. Martonchik, D. J. Diner, K. A. Crean, and B. Holben
563 (2005), Multiangle imaging spectroradiometer (MISR) global aerosol optical
564 depth validation based on 2 years of coincident aerosol robotic network
565 (AERONET) observations, *Journal of Geophysical Research-Atmospheres*, *110*,
566 D10S04, doi:10.1029/2004JD004706.
567 Kaufman, Y. J., D. Tanre, L. A. Remer, E. F. Vermote, A. Chu, and B. N. Holben (1997),
568 Operational remote sensing of tropospheric aerosol over land from EOS moderate
569 resolution imaging spectroradiometer, *Journal of Geophysical Research-*
570 *Atmospheres*, *102*, 17051-17067.

571 Kaufman, Y. J., P. V. Hobbs, V. Kirchhoff, P. Artaxo, L. A. Remer, B. N. Holben, M. D.
572 King, D. E. Ward, E. M. Prins, K. M. Longo, L. F. Mattos, C. A. Nobre, J. D.
573 Spinhirne, Q. Ji, A. M. Thompson, J. F. Gleason, S. A. Christopher, and S. C.
574 Tsay (1998), Smoke, clouds, and radiation - Brazil (SCAR-B) experiment,
575 *Journal of Geophysical Research-Atmospheres*, *103*, 31783-31808.
576 Kaufman, Y. J., D. Tanre, and O. Boucher (2002a), A satellite view of aerosols in the
577 climate system, *Nature*, *419*, 215-223.
578 Kaufman, Y. J., D. Tanre, B. N. Holben, S. Mattoo, L. A. Remer, T. F. Eck, J. Vaughan,
579 and B. Chatenet (2002b), Aerosol radiative impact on spectral solar flux at the
580 surface, derived from principal-plane sky measurements, *Journal of the*
581 *Atmospheric Sciences*, *59*, 635-646.
582 Kaufman, Y. J., L. A. Remer, D. Tanre, R. R. Li, R. Kleidman, S. Mattoo, R. C. Levy, T.
583 F. Eck, B. N. Holben, C. Ichoku, J. V. Martins, and I. Koren (2005), A critical
584 examination of the residual cloud contamination and diurnal sampling effects on
585 MODIS estimates of aerosol over ocean, *IEEE Transactions on Geoscience and*
586 *Remote Sensing*, *43*, 2886-2897.
587 Kiehl, J. T., and B. P. Briegleb (1993), The relative roles of sulfate aerosols and
588 greenhouse gases in climate forcing, *Science*, *260*, 311-314.
589 Kiladis, G. N., G. A. Meehl, and K. M. Weickmann (1994), Large-scale circulation
590 associated with westerly wind bursts and deep convection over the western
591 equatorial Pacific, *Journal of Geophysical Research-Atmospheres*, *99*, 18527-
592 18544.
593 Kiladis, G. N., K. H. Straub, G. C. Reid, and K. S. Gage (2001), Aspects of interannual
594 and intraseasonal variability of the tropopause and lower stratosphere, *Quarterly*
595 *Journal of the Royal Meteorological Society*, *127*, 1961-1983.
596 Kiladis, G. N., K. H. Straub, and P. T. Haertel (2005), Zonal and vertical structure of the
597 Madden-Julian oscillation, *Journal of the Atmospheric Sciences*, *62*, 2790-2809.

598 King, M. D., Y. J. Kaufman, D. Tanre, and T. Nakajima (1999), Remote sensing of
599 tropospheric aerosols from space: Past, present, and future, *Bulletin of the*
600 *American Meteorological Society*, *80*, 2229-2259.
601 Koch, D., J. Park, and A. Del Genio (2003), Clouds and sulfate are anticorrelated: A new
602 diagnostic for global sulfur models, *Journal of Geophysical Research-*
603 *Atmospheres*, *108*, 4781, doi:10.1029/2003JD003621.
604 Koren, I., Y. J. Kaufman, L. A. Remer, and J. V. Martins (2004), Measurement of the
605 effect of Amazon smoke on inhibition of cloud formation, *Science*, *303*, 1342-
606 1345.
607 Lau, K. M., and K. M. Kim (2006), Observational relationships between aerosol and
608 Asian monsoon rainfall, and circulation, *Geophysical Research Letters*, *33*,
609 L21810, doi:10.1029/2006GL027546.
610 Lau, W. K. M. (2005), ENSO connections, In *Intraseasonal variability of the*
611 *atmosphere-ocean climate system*, Edited by W. K. M. Lau and D. E. Waliser, pp.
612 436, Springer, Heidelberg, Germany.
613 Lau, W. K. M., and D. E. Waliser (2005), *Intraseasonal variability of the atmosphere-*
614 *ocean climate system*, Edited by W. K. M. Lau and D. E. Waliser, pp 474,
615 Springer, Heidelberg, Germany.
616 Levy, R. C., L. A. Remer, D. Tanre, Y. J. Kaufman, C. Ichoku, B. N. Holben, J. M.
617 Livingston, P. B. Russell, and H. Maring (2003), Evaluation of the moderate-
618 resolution imaging spectroradiometer (MODIS) retrievals of dust aerosol over the
619 ocean during PRIDE, *Journal of Geophysical Research-Atmospheres*, *108*, 8594,
620 doi:10.1029/2002JD002460.
621 Levy, R. C., L. A. Remer, J. V. Martins, Y. J. Kaufman, A. Plana-Fattori, J. Redemann,
622 and B. Wenny (2005), Evaluation of the MODIS aerosol retrievals over ocean and
623 land during CLAMS, *Journal of the Atmospheric Sciences*, *62*, 974-992.
624 Li, R. R., Y. J. Kaufman, W. M. Hao, J. M. Salmon, and B. C. Gao (2004), A technique

for detecting burn scars using MODIS data, *IEEE Transactions on Geoscience and Remote Sensing*, *42*, 1300-1308.

Lin, J. C., T. Matsui, R. A. Pielke, and C. Kummerow (2006), Effects of biomass-burning-derived aerosols on precipitation and clouds in the Amazon basin: A satellite-based empirical study, *Journal of Geophysical Research-Atmospheres*, *111*, D19204, doi:10.1029/2005JD006884.

Lin, X., and R. H. Johnson (1996), Kinematic and thermodynamic characteristics of the flow over the western Pacific warm pool during TOGA COARE, *Journal of the Atmospheric Sciences*, *53*, 695-715.

Madden, R. A., and P. R. Julian (1971), Detection of a 40-50 day oscillation in the zonal wind in the tropical Pacific, *Journal of the Atmospheric Sciences*, *28*, 702-708.

Madden, R. A., and P. R. Julian (1994), Observations of the 40-50-day tropical oscillation - a review, *Monthly Weather Review*, *122*, 814-837.

Madden, R. A., and P. R. Julian (2005), Historical perspective, In *Intraseasonal variability of the atmosphere-ocean climate system*, Edited by W. K. M. Lau and D. E. Waliser, pp. 474, Springer, Heidelberg, Germany.

Mahowald, N., C. Luo, J. del Corral, and C. S. Zender (2003), Interannual variability in atmospheric mineral aerosols from a 22-year model simulation and observational data, *Journal of Geophysical Research-Atmospheres*, *108*, 4352, doi:10.1029/2002JD002821.

Maloney, E. D., and D. L. Hartmann (2000), Modulation of hurricane activity in the Gulf of Mexico by the Madden-Julian oscillation, *Science*, *287*, 2002-2004.

Martins, J. V., D. Tanre, L. Remer, Y. Kaufman, S. Mattoo, and R. Levy (2002), MODIS cloud screening for remote sensing of aerosols over oceans using spatial variability, *Geophysical Research Letters*, *29*, 1619, doi:10.1029/2001GL013252.

Martonchik, J. V., D. J. Diner, K. A. Crean, and M. A. Bull (2002), Regional aerosol retrieval results from MISR, *IEEE Transactions on Geoscience and Remote*

652 *Sensing*, *40*, 1520-1531.
653 McPhaden, M. J. (1999), Genesis and evolution of the 1997-98 El Niño, *Science*, *283*,
654 950-954.
655 Mishchenko, M. I., I. V. Geogdzhayev, B. Cairns, W. B. Rossow, and A. A. Lacis (1999),
656 Aerosol retrievals over the ocean by use of channels 1 and 2 AVHRR data:
657 Sensitivity analysis and preliminary results, *Applied Optics*, *38*, 7325-7341.
658 Mishchenko, M. I., and I. V. Geogdzhayev (2007), Satellite remote sensing reveals
659 regional tropospheric aerosol trends, *Optics Express*, *15*, 7423-7438.
660 Myhre, G., F. Stordal, M. Johnsrud, A. Ignatov, M. I. Mischenko, I. V. Geogdzhayev, D.
661 Tanre, J. L. Deuze, P. Goloub, T. Nakajima, A. Higurashi, O. Torres, and B.
662 Holben (2004), Intercomparison of satellite retrieved aerosol optical depth over
663 the ocean, *Journal of the Atmospheric Sciences*, *61*, 499-513.
664 Myhre, G., F. Stordal, M. Johnsrud, D. J. Diner, I. V. Geogdzhayev, J. M. Haywood, B.
665 N. Holben, T. Holzer-Popp, A. Ignatov, R. A. Kahn, Y. J. Kaufman, N. Loeb, J.
666 V. Martonchik, M. I. Mishchenko, N. R. Nalli, L. A. Remer, M. Schroedter-
667 Homscheidt, D. Tanre, O. Torres, and M. Wang (2005), Intercomparison of
668 satellite retrieved aerosol optical depth over ocean during the period September
669 1997 to December 2000, *Atmospheric Chemistry and Physics*, *5*, 1697-1719.
670 Ramanathan, V., P. J. Crutzen, J. T. Kiehl, and D. Rosenfeld (2001a), Atmosphere -
671 aerosols, climate, and the hydrological cycle, *Science*, *294*, 2119-2124.
672 Ramanathan, V., P. J. Crutzen, J. Lelieveld, A. P. Mitra, D. Althausen, J. Anderson, M.
673 O. Andreae, W. Cantrell, G. R. Cass, C. E. Chung, A. D. Clarke, J. A. Coakley,
674 W. D. Collins, W. C. Conant, F. Dulac, J. Heintzenberg, A. J. Heymsfield, B.
675 Holben, S. Howell, J. Hudson, A. Jayaraman, J. T. Kiehl, T. N. Krishnamurti, D.
676 Lubin, G. McFarquhar, T. Novakov, J. A. Ogren, I. A. Podgorny, K. Prather, K.
677 Priestley, J. M. Prospero, P. K. Quinn, K. Rajeev, P. Rasch, S. Rupert, R.
678 Sadourny, S. K. Satheesh, G. E. Shaw, P. Sheridan, and F. P. J. Valero (2001b),

679 Indian ocean experiment: An integrated analysis of the climate forcing and effects
680 of the great Indo-Asian haze, *Journal of Geophysical Research-Atmospheres*, *106*,
681 28371-28398.
682 Ramanathan, V., C. Chung, D. Kim, T. Bettge, L. Buja, J. T. Kiehl, W. M. Washington,
683 Q. Fu, D. R. Sikka, and M. Wild (2005), Atmospheric brown clouds: Impacts on
684 south Asian climate and hydrological cycle, *Proceedings of the National Academy*
685 *of Sciences of the United States of America*, *102*, 5326-5333.
686 Redemann, J., P. B. Russell, and P. Hamill (2001), Dependence of aerosol light
687 absorption and single-scattering albedo on ambient relative humidity for sulfate
688 aerosols with black carbon cores, *Journal of Geophysical Research-Atmospheres*,
689 *106*, 27485-27495.
690 Remer, L. A., D. Tanre, Y. J. Kaufman, C. Ichoku, S. Mattoo, R. Levy, D. A. Chu, B.
691 Holben, O. Dubovik, A. Smirnov, J. V. Martins, R. R. Li, and Z. Ahmad (2002),
692 Validation of MODIS aerosol retrieval over ocean, *Geophysical Research Letters*,
693 *29*, 1618, 10.1029/2001GL013204.
694 Remer, L. A., Y. J. Kaufman, D. Tanre, S. Mattoo, D. A. Chu, J. V. Martins, R. R. Li, C.
695 Ichoku, R. C. Levy, R. G. Kleidman, T. F. Eck, E. Vermote, and B. N. Holben
696 (2005), The MODIS aerosol algorithm, products, and validation, *Journal of the*
697 *Atmospheric Sciences*, *62*, 947-973.
698 Rosenfeld, D. (1999), TRMM observed first direct evidence of smoke from forest fires
699 inhibiting rainfall, *Geophysical Research Letters*, *26*, 3105-3108.
700 Rosenfeld, D. (2000), Suppression of rain and snow by urban and industrial air pollution,
701 *Science*, *287*, 1793-1796.
702 Rossow, W. B., and L. C. Garder (1993), Cloud detection using satellite measurements of
703 infrared and visible radiances for ISCCP, *Journal of Climate*, *6*, 2341-2369.
704 Rossow, W. B., and R. A. Schiffer (1999), Advances in understanding clouds from
705 ISCCP, *Bulletin of the American Meteorological Society*, *80*, 2261-2287.

706 Rui, H., and B. Wang (1990), Development characteristics and dynamic structure of
707 tropical intraseasonal convection anomalies, *Journal of the Atmospheric Sciences*,
708 *47*, 357-379.
709 Satheesh, S. K., and V. Ramanathan (2000), Large differences in tropical aerosol forcing
710 at the top of the atmosphere and earth's surface, *Nature*, *405*, 60-63.
711 Seinfeld, J. H., G. R. Carmichael, R. Arimoto, W. C. Conant, F. J. Brechtel, T. S. Bates,
712 T. A. Cahill, A. D. Clarke, S. J. Doherty, P. J. Flatau, B. J. Huebert, J. Kim, K. M.
713 Markowicz, P. K. Quinn, L. M. Russell, P. B. Russell, A. Shimizu, Y. Shinozuka,
714 C. H. Song, Y. Tang, I. Uno, A. M. Vogelmann, R. J. Weber, J.-H. Woo, and X.
715 Y. Zhang (2004), ACE-ASIA: Regional climatic and atmospheric chemical
716 effects of Asian dust and pollution, *Bulletin of the American Meteorological*
717 *Society*, *85*, 367-380.
718 Smirnov, A., B. N. Holben, T. F. Eck, O. Dubovik, and I. Slutsker (2000), Cloud-
719 screening and quality control algorithms for the AERONET database, *Remote*
720 *Sensing of Environment*, *73*, 337-349.
721 Tanre, D., Y. J. Kaufman, M. Herman, and S. Mattoo (1997), Remote sensing of aerosol
722 properties over oceans using the MODIS/EOS spectral radiances, *Journal of*
723 *Geophysical Research-Atmospheres*, *102*, 16971-16988.
724 Tian, B. J., D. E. Waliser, and E. J. Fetzer (2006a), Modulation of the diurnal cycle of
725 tropical deep convective clouds by the MJO, *Geophysical Research Letters*, *33*,
726 L20704, doi:10.1029/2006GL027752.
727 Tian, B. J., D. E. Waliser, E. J. Fetzer, B. H. Lambrigtsen, Y. L. Yung, and B. Wang
728 (2006b), Vertical moist thermodynamic structure and spatial-temporal evolution
729 of the MJO in AIRS observations, *Journal of the Atmospheric Sciences*, *63*, 2462-
730 2485.
731 Tian, B. J., Y. L. Yung, D. E. Waliser, T. Tyranowski, L. Kuai, E. J. Fetzer, and F. W.
732 Irion (2007), Intraseasonal variations of the tropical total ozone and their

733 connection to the Madden-Julian oscillation, *Geophysical Research Letters*, *34*,
734 L08704, doi:10.1029/2007GL029451.
735 Torres, O., P. K. Bhartia, J. R. Herman, Z. Ahmad, and J. Gleason (1998), Derivation of
736 aerosol properties from satellite measurements of backscattered ultraviolet
737 radiation: Theoretical basis, *Journal of Geophysical Research-Atmospheres*, *103*,
738 17099-17110.
739 Torres, O., A. Tanskanen, B. Veihelman, C. Ahn, R. Braak, P. K. Bhartia, P. Veefkind,
740 and P. Levelt (2007), Aerosols and surface UV products from OMI observations:
741 An overview, *Journal of Geophysical Research-Atmospheres*, *112*, in press.
742 Twomey, S. A., M. Piepgrass, and T. L. Wolfe (1984), An assessment of the impact of
743 pollution on global cloud albedo, *Tellus Series B-Chemical and Physical*
744 *Meteorology*, *36*, 356-366.
745 Vecchi, G. A., and N. A. Bond (2004), The Madden-Julian oscillation (MJO) and
746 northern high latitude wintertime surface air temperatures, *Geophysical Research*
747 *Letters*, *31*, L04104, doi:10.1029/2003GL018645.
748 Waliser, D. E., R. Murtugudde, and L. Lucas (2003), Indo-Pacific ocean response to
749 atmospheric intraseasonal variability. Part I: Austral summer and the Madden-
750 Julian oscillation, *Journal of Geophysical Research-Oceans*, *108*,
751 10.1029/2002JC001620.
752 Waliser, D. E. (2006a), Predictability of tropical intraseasonal variability, In
753 *Predictability of weather and climate*, Edited by T. N. Palmer and R. Hagedorn,
754 pp. 718, Cambridge University Press, New York.
755 Waliser, D. E. (2006b), Intraseasonal variability, In *The Asian monsoon*, Edited by B.
756 Wang, pp. 787, Springer, Heidelberg, Germany.
757 Wang, B., and H. Rui (1990), Synoptic climatology of transient tropical intraseasonal
758 convection anomalies - 1975-1985, *Meteorology and Atmospheric Physics*, *44*,
759 43-61.

760 Wheeler, M. C., and J. L. McBride (2005), Australian-Indonesian monsoon, In
761 *Intraseasonal variability of the atmosphere-ocean climate system*, Edited by W.
762 K. M. Lau and D. E. Waliser, pp. 436, Springer, Heidelberg, Germany.
763 Wilcox, E. M., and V. Ramanathan (2004), The impact of observed precipitation upon
764 the transport of aerosols from south Asia, *Tellus Series B-Chemical and Physical*
765 *Meteorology*, *56*, 435-450.
766 Winker, D. M., J. Pelon, and M. P. McCormick (2003), The CALIPSO mission:
767 Spaceborne lidar for observation of aerosols and clouds, *Proceedings of the*
768 *Society of Photo-Optical Instrumentation Engineers*, *4893*, 1–11.
769 Winker, D. M., W. H. Hunt, and C. A. Hostetler (2004), Status and performance of the
770 CALIOP lidar, *Proceedings of the Society of Photo-Optical Instrumentation*
771 *Engineers*, *5575*, 8-15.
772 Wong, S., and A. E. Dessler (2007), Regulation of H2O and CO in tropical tropopause
773 layer by the Madden-Julian oscillation., *Journal of Geophysical Research-*
774 *Atmospheres*, in press.
775 Xie, P. P., and P. A. Arkin (1997), Global precipitation: A 17-year monthly analysis
776 based on gauge observations, satellite estimates, and numerical model outputs,
777 *Bulletin of the American Meteorological Society*, *78*, 2539-2558.
778 Yasunari, T. (1980), A quasi-stationary appearance of the 30-40 day period in the
779 cloudiness fluctuations during the summer monsoon over India., *Journal of the*
780 *Meteorological Society of Japan*, *59*, 336-354.
781 Yu, H., Y. J. Kaufman, M. Chin, G. Feingold, L. A. Remer, T. L. Anderson, Y.
782 Balkanski, N. Bellouin, O. Boucher, S. Christopher, P. DeCola, R. Kahn, D.
783 Koch, N. Loeb, M. S. Reddy, M. Schulz, T. Takemura, and M. Zhou (2006), A
784 review of measurement-based assessments of the aerosol direct radiative effect
785 and forcing, *Atmospheric Chemistry and Physics*, *6*, 613-666.
786 Ziemke, J. R., and S. Chandra (2003), A Madden-Julian oscillation in tropospheric ozone,

787 *Geophysical Research Letters*, *30*, 2182, doi:10.1029/2003GL018523.

788

789
790

Figure Captions

Figure 1: The dates (indicated by x) of selected MJO events for TOMS (26, from Jan 1980 to Dec 1992), MODIS (13, from Feb 2000 to Jun 2005), and AVHRR (48, from Jan 1982 to May 2005) periods based on the amplitude pentad time series for the first EEOF mode of CMAP rainfall anomaly from NH wintertime (Nov–Apr) and the region 30°S–30°N and 30°E–150°W. Three dashed lines show the EEOF amplitude of ±1 and 0. The solid colored lines indicate the start and end of each aerosol data record (blue for TOMS, red for MODIS, and green for AVHRR).

Figure 2: Composite maps of the TOMS AI anomalies (color shading) associated with the MJO indicated by the CMAP rainfall anomalies (contours). TOMS AI anomalies are only plotted if they exceed 95% confidence limit using a student t-test.

Figure 3: As in Figure 2, except for MODIS AOT.

Figure 4: The zero-lag correlation between the MJO composite CMAP rainfall anomalies and the MJO composite aerosol anomalies (shown in Figures 2 & 3) from the three satellite aerosol products (i.e., TOMS AI MODIS AOT, and AVHRR AOT).

Figure 5: The MJO composite CMAP rainfall anomalies and AERONET AOT at two AERONET sites: Kaashidoo and Nauru. The TOMS AI, MODIS AOT, and AVHRR AOT at the nearby grids are also included for comparison.

811

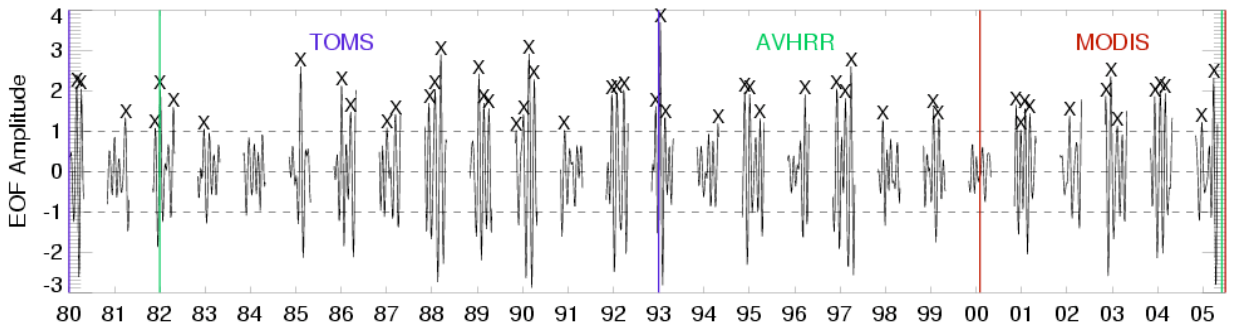

Figure 1: The dates (indicated by x) of selected MJO events for TOMS (26, from Jan 1980 to Dec 1992), MODIS (13, from Feb 2000 to Jun 2005), and AVHRR (48, from Jan 1982 to May 2005) periods based on the amplitude pentad time series for the first EEOF mode of CMAP rainfall anomaly from NH wintertime (Nov–Apr) and the region 30°S–30°N and 30°E–150°W. Three dashed lines show the EEOF amplitude of ±1 and 0. The solid colored lines indicate the start and end of each aerosol data record (blue for TOMS, red for MODIS, and green for AVHRR).

812

813

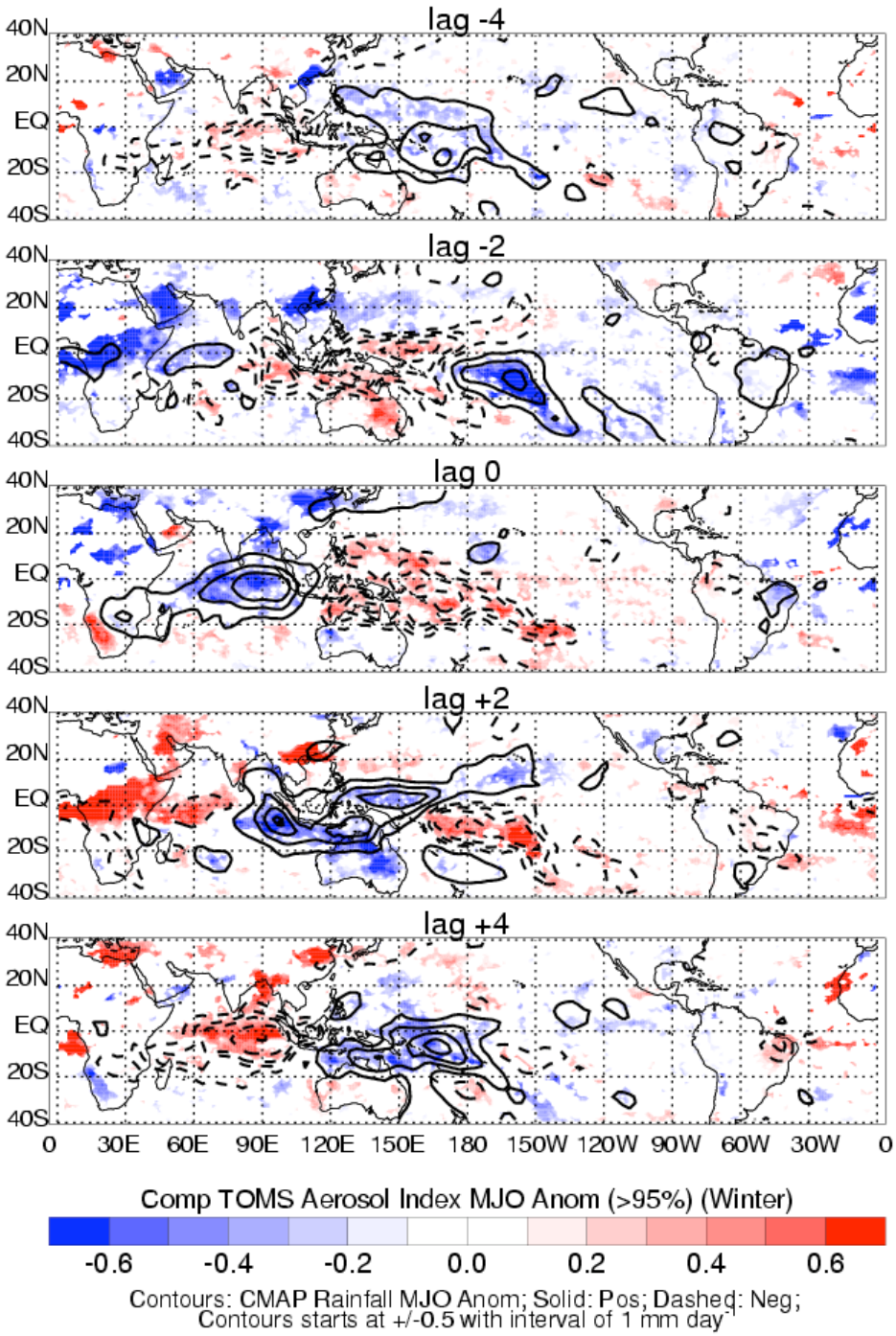

Figure 2: Composite maps of the TOMS AI anomalies (color shading) associated with the MJO indicated by the CMAP rainfall anomalies (contours). TOMS AI anomalies are only plotted if they exceed 95% confidence limit using a student t-test.

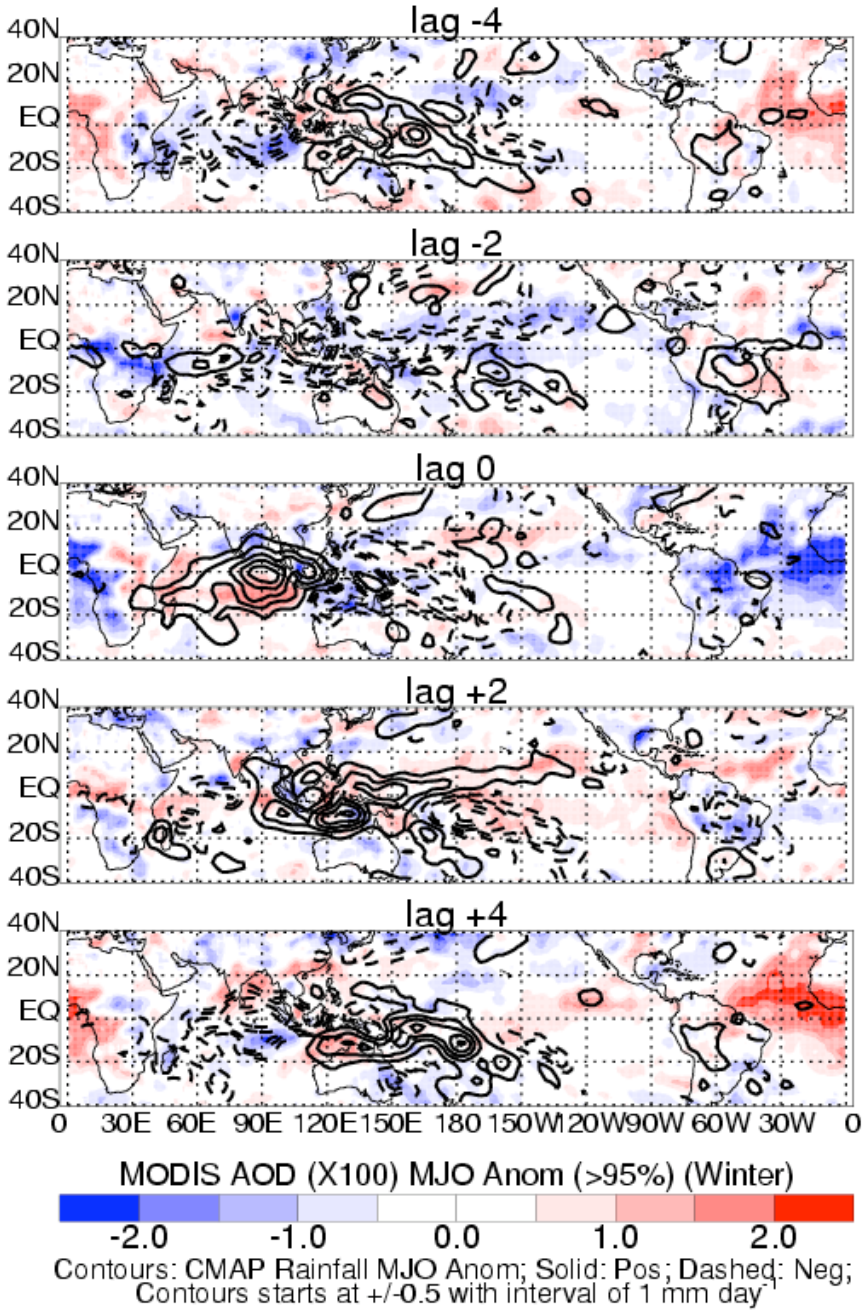

Figure 3: As in Figure 2, except for MODIS AOT.

816

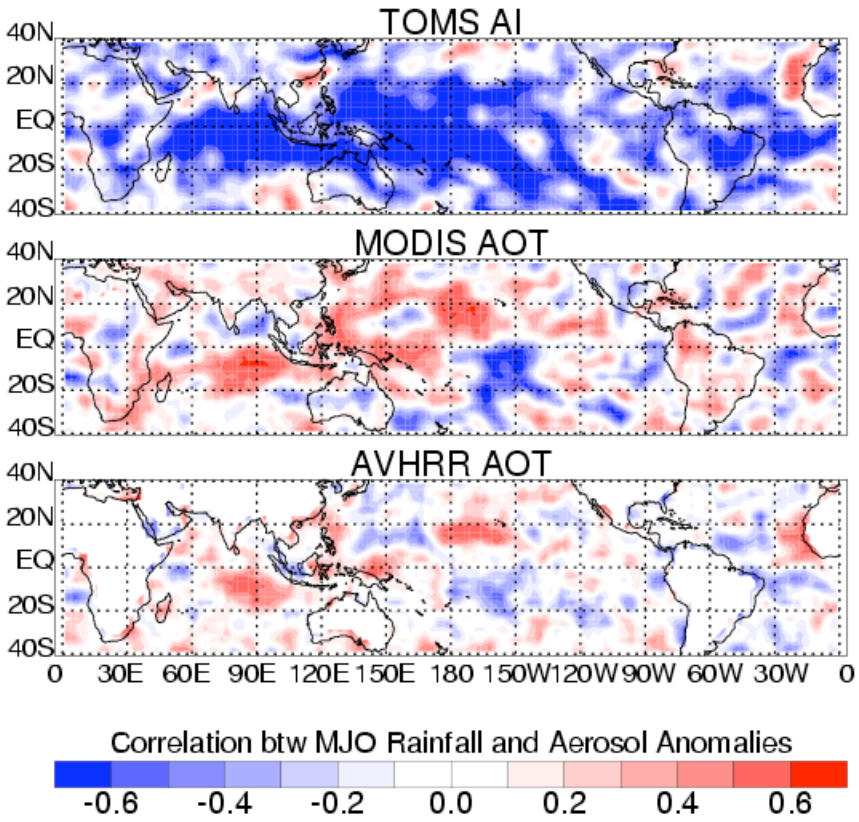

Figure 4: The zero-lag correlation between the MJO composite CMAP rainfall anomalies and the MJO composite aerosol anomalies (shown in Figures 2 & 3) from the three satellite aerosol products (i.e., TOMS AI, MODIS AOT, and AVHRR AOT).

817

818

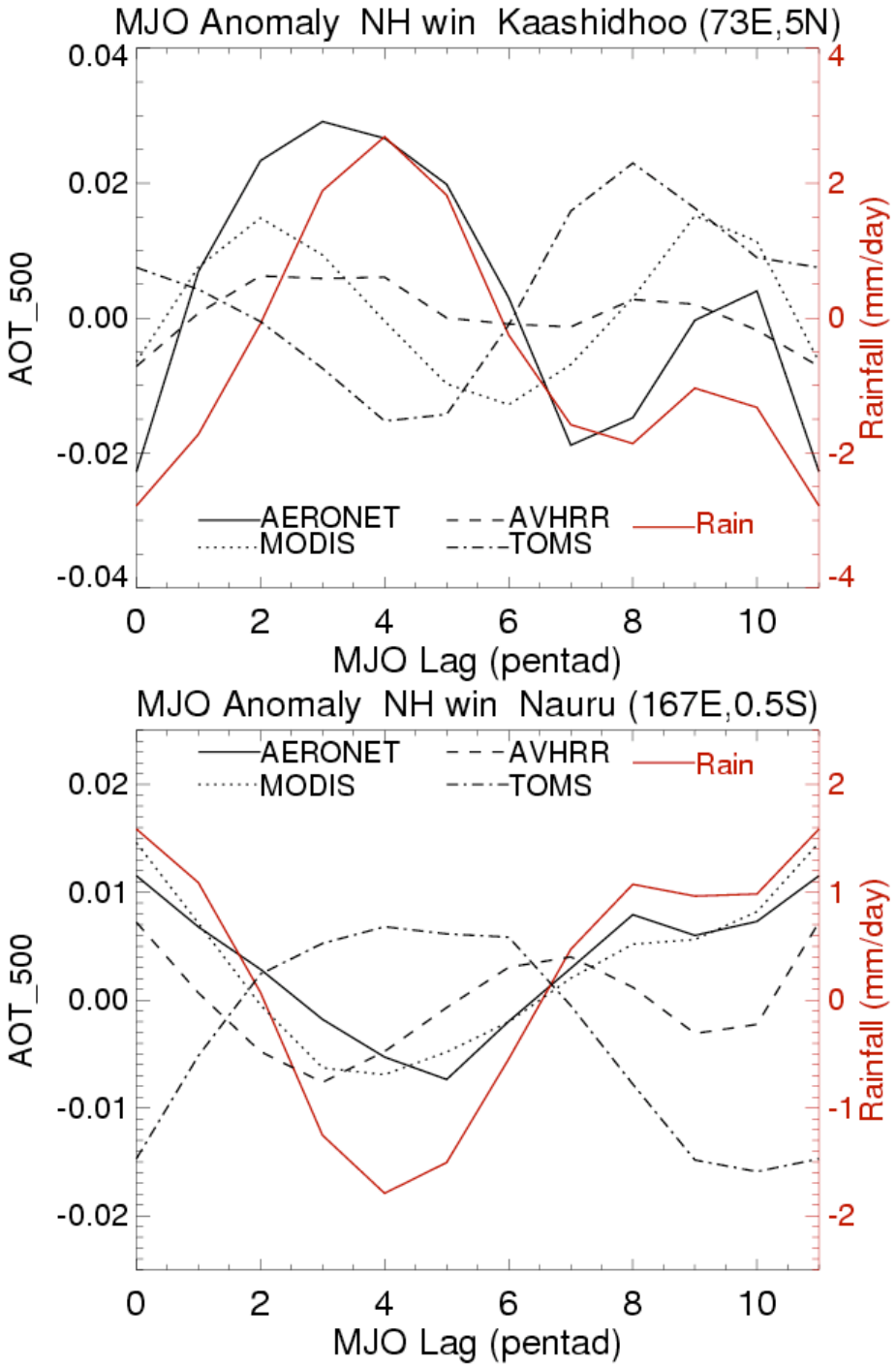

Figure 5: The MJO composite CMAP rainfall anomalies and AERONET AOT at two AERONET sites: Kaashidoo and Nauru. The TOMS AI, MODIS AOT, and AVHRR AOT at the nearby grids are also included for comparison.